Physica B 407 (2012) 4793–4796

Contents lists available at SciVerse ScienceDirect

Physica B

journal homepage: www.elsevier.com/locate/physb

The structural and multiferroic properties of $(Bi_{1-x}La_x)(Fe_{0.95}Co_{0.05})O_3$ ceramics

Qingyu Xu [a,b,*], Xiaohong Zheng [a], Liaoyu Wang [c], Yan Zhang [a], Dunhui Wang [c], Mingxiang Xu [a]

[a] Department of Physics, Southeast University, Nanjing, Jiangsu 211189, China
[b] Key Laboratory of MEMS of the Ministry of Education, Southeast University, Nanjing 210096, China
[c] Department of Physics, Nanjing University, Nanjing 210008, China

ARTICLE INFO

Article history:
Received 12 April 2012
Received in revised form
14 August 2012
Accepted 5 September 2012
Available online 16 September 2012

Keywords:
Multiferroics
$BiFeO_3$
Raman

ABSTRACT

La and Co co-doped $BiFeO_3$ ($(Bi_{1-x}La_x)(Fe_{0.95}Co_{0.05})O_3$ ($x=0$, 0.10, 0.20, 0.30)) ceramics were prepared by tartaric acid modified sol–gel method. The X-ray diffraction patterns indicate a transition from rhombohedral structure to tetragonal structure at $x=0.20$, which has been confirmed by the Raman measurements. The band gap increases with increasing x to 0.20, and then decreases with further increasing x to 0.30. The structural transition has significant effects on the multiferroic properties. The remnant magnetization and saturate ferromagnetic magnetization decrease abruptly with increasing x to 0.10, and then gradually increase with further increasing x up to 0.30. The coercivity is significantly reduced with increasing La doping concentration. The ferroelectricity has been improved by La doping, and the polarization increases with increasing x to 0.10, then decreases with further increasing x up to 0.30. The simultaneous coexistence of soft ferromagnetism and ferroelectricity at room temperature in tetragonal $Bi_{0.70}La_{0.30}Fe_{0.95}Co_{0.05}O_3$ indicates the potential multiferroic applications.

1. Introduction

Multiferroic materials posses the magnetoelectric effect (ME) which allows the coupling between the ferroic orderings, such as ferromagnetism, ferroelectricity, etc., making them promising candidates for applications in memories, spintronics and magnetoelectric sensor devices [1,2]. Among the rare multiferroic materials, $BiFeO_3$ is one of the well-known single-phase multiferroic materials with G-type antiferromagnetic behavior below Neel temperature $T_N \sim 643$ K and ferroelectric behavior below Curie temperature $T_C \sim 1103$ K [3]. In bulk form, $BiFeO_3$ has a rhombohedrally distorted perovskite structure with space group $R3c$ [3]. The observation of large polarization in epitaxial $BiFeO_3$ thin films, polycrystalline films and single crystals has made this system especially promising for applications [1,4,5]. However, due to the antiferromagnetism with cycloidal spin structure in bulk $BiFeO_3$, the magnetization is rather modest [6]. Furthermore, the large leakage current is still a main drawback which limits the ME applications of $BiFeO_3$.

Much work has been done to suppress the leakage current and enhance the ferromagnetism by means of doping ions in $BiFeO_3$ [7–9]. It has been suggested that the conductivity and ferroelectric hysteresis loop in $BiFeO_3$ may be strongly affected by the reduction of Fe^{3+} to Fe^{2+} [10,11]. Attempts have been made to suppress the leakage current by substituting Bi^{3+} with La^{3+} and Nd^{3+} [12]. It is thought that vacancies created by the removal of Bi^{3+} ions are compensated by the substitution of rare earth ions, reducing the conductivity. Replacing Fe^{3+} ions with Ni^{2+} ions increases the leakage current [13]. Conversely, substituting other transition metal (TM) ions such as Ti^{4+}, Mn^{3+} is expected to increase the resistance by reducing valence fluctuations in Fe^{3+} [13–15]. Additionally, doping with magnetic TM ions has been observed to significantly improve the magnetic properties of $BiFeO_3$ [16–18], which has been ascribed to the ferrimagnetic coupling between Fe^{3+} and the doped magnetic ions [18,19]. Among the 3d TM ions doping in $BiFeO_3$, the Co ions are the best for both enhancing the magnetization and keeping the clear ferroelectricity. However, the coercivity of the magnetic hysteresis loop is still quite large, which hinders its applications in spintronics where a small magnetic field should be applied to switch the magnetization [18]. The strategy of Fe- and Bi-site co-doping might be an efficient way to improve the ferroelectric and ferromagnetic properties of $BiFeO_3$, since it combines the modifications of structure and magnetic exchange interaction. In this paper, La^{3+} and Co^{3+} ions were introduced in Bi-site and Fe-site, respectively. The structural, magnetic and ferroelectric properties of La-doped $Bi(Fe_{0.95}Co_{0.05})O_3$ were systematically investigated.

2. Experimental

$(Bi_{1-x}La_x)(Fe_{0.95}Co_{0.05})O_3$ ($x=0$, 0.10, 0.20, 0.30) ceramics were prepared by tartaric acid modified sol–gel method. Appropriate

* Corresponding author at: Southeast University Department of Physics Jiangning Nanjing, Jiangsu 211189, China.
Tel. +86 2552090600x8308; fax: +86 2552090600x8203.
E-mail address: xuqingyu@seu.edu.cn (Q. Xu).

0921-4526/$ - see front matter © 2012 Elsevier B.V. All rights reserved.
http://dx.doi.org/10.1016/j.physb.2012.09.021

amounts of $Bi(NO_3)_3 \cdot 5H_2O$, $Fe(NO_3)_3 \cdot 9H_2O$, $Co(NO_3)_2 \cdot 6H_2O$, and $La(NO_3)_3 \cdot nH_2O$ were dissolved in diluted HNO_3 solution. Tartaric acid in 1:1 M ratio with respect to metal nitrates was added to the solution. The obtained solutions were dried at 80 °C, and then calcined at 600 °C in air for 2 h. The obtained powders were grinded, put into the oven and calcined at 600 °C in air for 2 h once again. The structures of samples were studied by X-ray diffraction (XRD) with Cu K_α radiation. The optical properties were measured by UV-2450. Raman measurements were carried out on a Horiba Jobin Yvon LabRAM HR 800 micro-Raman spectrometer with 785 nm excitation source under air ambient condition at room temperature. The laser focused on the sample surface in diameter of 1 μm. The magnetization of the samples was measured by a vibrating sample magnetometer integrated in a physical property measurement system (PPMS-9, Quantum Design). For ferroelectricity measurements, the powders were grinded and pressed into 1 mm thick disks in diameter of 13 mm. The disks were directly put into an 800 °C oven and sintered in air for 2 h. And the ferroelectric properties were measured by a Radiant Ferroelectric tester (Radiant Technologies, USA).

3. Results and discussions

Fig. 1 shows the XRD patterns of $(Bi_{1-x}La_x)(Fe_{0.95}Co_{0.05})O_3$ ($x=0$, 0.10, 0.20, 0.30) ceramics. Except for the main peaks which can be indexed to $BiFeO_3$, extra peaks were observed in the XRD patterns, which are identified to be the impurity phases of $Bi_2Fe_4O_9$ and $Bi_{25}FeO_{39}$. It should be noted that the intensity of the diffraction peaks from the impurities in the samples with $x=0.10$, 0.20, 0.30 is weaker than those in $BiFe_{0.95}Co_{0.05}O_3$. This suggests that doping with La may suppress the formation of the secondary phases, which is consistent with our previous work [20]. With distorted rhombohedral structure ($R3c$), $Bi(Fe_{0.95}Co_{0.05})O_3$ showed the peak splitting in XRD pattern that appears at 31°–33°, 38.5°–40.5°, 51°–52°, and 57–58° of 2θ values [21,22]. The splitting peaks start to merge together with increasing La concentration, indicating the gradual transition from rhombohedral to tetragonal structure. As can be seen, the merger of the splitting peaks almost finishes with La substitution concentration of 0.20, indicating that the structure of ceramics changes from rhombohedral to tetragonal symmetry is almost complete at $x=0.20$ [23].

The Raman spectra of $(Bi_{1-x}La_x)(Fe_{0.95}Co_{0.05})O_3$ ($x=0$, 0.10, 0.20, 0.30) ceramics are shown in Fig. 2. Group theory predicts that $BiFeO_3$, a highly rhombohedrally distorted perovskite with $R3c$ space group, should have 13 ($4A_1+9E$) Raman active modes. However, not all the modes can be clearly resolved at room temperature, as shown in Fig. 2(e) [24]. The clearly resolved Raman modes of $Bi(Fe_{0.95}Co_{0.05})O_3$ are marked by arrows in Fig. 2, which further confirm the $R3c$ structure. In contrast to the Raman spectrum of $BiFeO_3$, the intensity of the E-9 mode of $Bi(Fe_{0.95}Co_{0.05})O_3$ is more prominent, which can be attributed to the distortion of $[(Co, Fe)^{3+}O_6]$ octahedral (i.e., Jahn–Teller distortion) due to the substitution of Fe^{3+} by Co^{3+}, as similar phenomenon has been observed in Mn-doped $BiFeO_3$ [25]. With increasing x, the intensity of the phonon modes of A_1–1 and A_1–2 decreases and the two modes merge together, confirming the transition from rhombohedral to tetragonal structure [25].

Fig. 3 shows the UV–visible optical diffuse reflectance spectra of $(Bi_{1-x}La_x)(Fe_{0.95}Co_{0.05})O_3$ ($x=0$, 0.10, 0.20, 0.30) ceramics. For the purpose of analysis, the diffuse reflectance, R of the sample can be related to the Kubelka–Munk function $F(R)=(1-R)^2/2R$. Extrapolation of linear region of these plots to $F(R)^2=0$ gives the corresponding direct energy band gap [26]. It is evident from Fig. 3 that the band gap for $(Bi_{1-x}La_x)(Fe_{0.95}Co_{0.05})O_3$ with $x=0$, 0.10, 0.20, 0.30 are 1.98 eV, 2.03 eV, 2.19 eV, and 2.06 eV, respectively, which are smaller than the reported value of about 2.34 eV for $BiFeO_3$ [27]. When $x \leq 0.20$, the band gap for the samples increases with increasing the La^{3+} concentration, and when $x=0.30$, the band gap decreases abruptly. This might be due to the compensation of the lattice distortion by the La^{3+} doping on

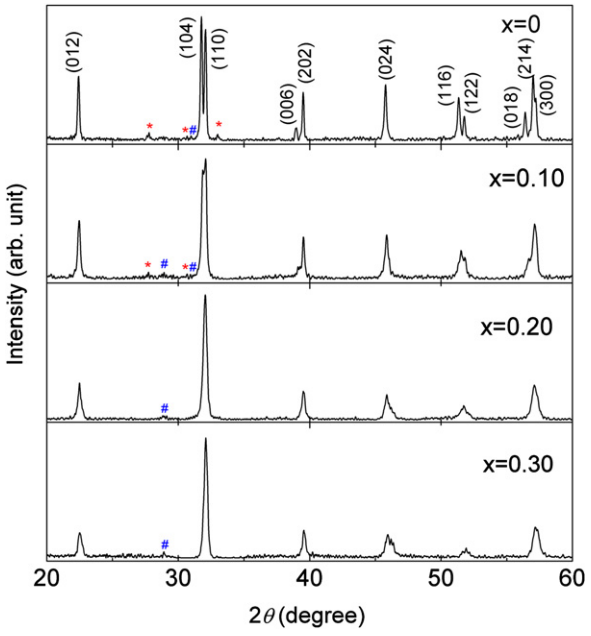

Fig. 1. XRD patterns of $(Bi_{1-x}La_x)(Fe_{0.95}Co_{0.05})O_3$ ($x=0$, 0.10, 0.20, 0.30) ceramics. The "*" and "#" mark the impurities of $Bi_{25}FeO_{39}$ and $Bi_2Fe_4O_9$, respectively.

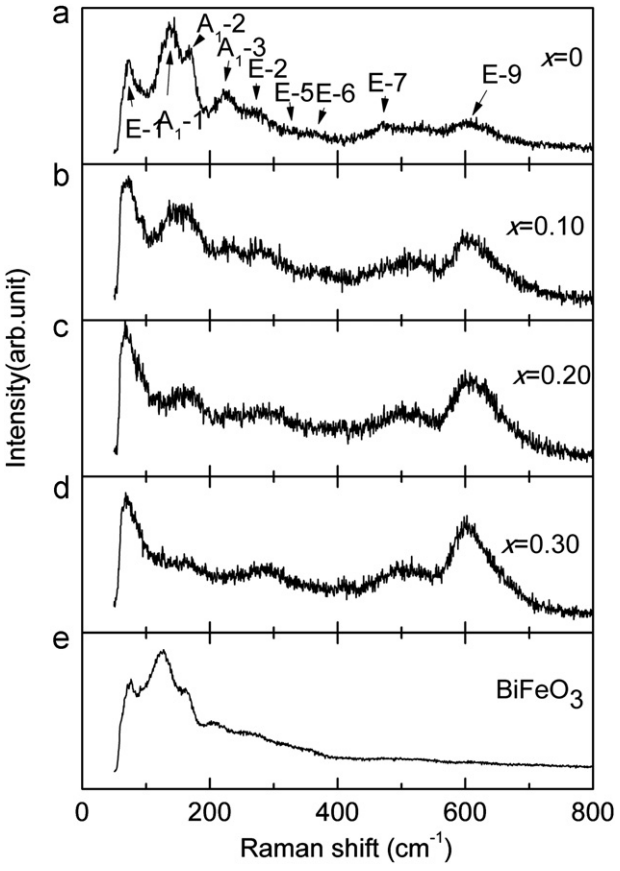

Fig. 2. Room temperature Raman spectra of $(Bi_{1-x}La_x)(Fe_{0.95}Co_{0.05})O_3$ ($x=0$, 0.10, 0.20, 0.30) ceramics. The Raman spectrum of $BiFeO_3$ is shown as reference.

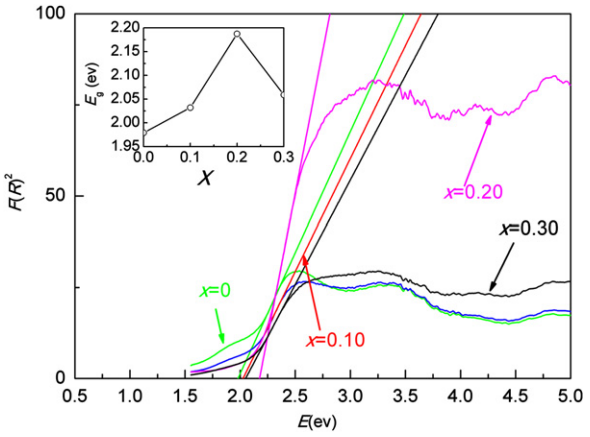

Fig. 3. Room temperature diffuse reflectance spectra of $(Bi_{1-x}La_x)(Fe_{0.95}Co_{0.05})O_3$ (x=0, 0.10, 0.20, 0.30) ceramics. The inset shows the variation of band gap with x.

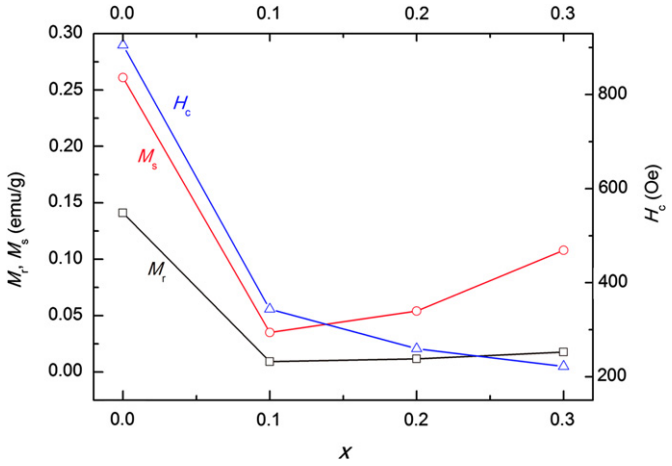

Fig. 5. The variation of M_s, M_r, and H_c as the function of La concentration x.

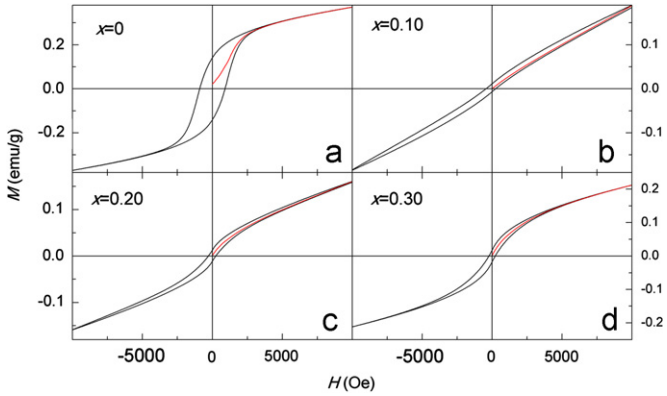

Fig. 4. The room temperature magnetic hysteresis loops of $(Bi_{1-x}La_x)(Fe_{0.95}Co_{0.05})O_3$ (x=0, 0.10, 0.20, 0.30) ceramics.

Bi^{3+} sites and Co^{3+} on Fe^{3+} sites, as the ionic radius of La^{3+} (1.172 Å) is larger than that of Bi^{3+} (1.17 Å), while the ionic radius of Co^{3+} (0.685 Å) is smaller than that of Fe^{3+} (0.69 Å) [28]. Thus, the La^{3+} substitution might expand the lattice, while Co^{3+} substitution might compress the lattice of $BiFeO_3$.

The magnetic hysteresis loops measured at room temperature for $(Bi_{1-x}La_x)(Fe_{0.95}Co_{0.05})O_3$ (x=0, 0.10, 0.20, 0.30) ceramics are shown in Fig. 4 which exhibit the weak ferromagnetism. The incorporation of La^{3+} ions into the $Bi(Fe_{0.95}Co_{0.05})O_3$ structure decreases the magnetization first with increasing La concentration to 0.10, and then increase with further increasing La concentration. The remnant magnetization (M_r) values are 0.141 emu/g, 0.0069 emu/g, 0.0108 emu/g, and 0.0177 emu/g for $(Bi_{1-x}La_x)(Fe_{0.95}Co_{0.05})O_3$ (x=0, 0.10, 0.20, 0.30), respectively. From the hysteresis loops, the samples show clear combination of paramagnetism and ferromagnetism. The ferromagnetic magnetization can be obtained by subtracting the paramagnetic contribution from the high field linear part. The saturate ferromagnetic magnetizations (M_s) are 0.261 emu/g, 0.035 emu/g, 0.054 emu/g, and 0.108 emu/g for $(Bi_{1-x}La_x)(Fe_{0.95}Co_{0.05})O_3$ (x=0, 0.10, 0.20, 0.30), respectively. The M_s and M_r as the function of x are plotted in Fig. 5.

The XRD and Raman measurements show that the incorporation of La^{3+} ions in Co-doped $BiFeO_3$ modifies the structure from rhombohedral to tetragonal. The sudden decrease of the magnetization with increasing La doping concentration to 0.10 might be related to this structural transition due to that the recent neutron diffraction results indicate the collinear antiferromagnetic spin arrangements in tetragonal $BiFeO_3$ [29,30]. Another possible explanation might be due to the opposite influence on the lattice distortion of La^{3+} substitution and Co^{3+} substitution. As the observed magnetization in $BiFeO_3$ mainly originate from the suppression of the cycloidal spin structure due to the lattice distortion, a compensation of the lattice distortion due to La^{3+} and Co^{3+} co-substitution may happen, leading to the sudden drop of the magnetization, similar to the recent report on the magnetization of $Bi_{0.8}La_{0.2-x}Pb_xFeO_3$ that La and Pb have the opposite effect on the magnetization enhancement of $BiFeO_3$ [31]. The increase of M_s and M_r with increasing $x \geq 0.10$ might be due to the ferrimagnetic exchange interaction between Fe^{3+} and Co^{3+} ions. The main contribution to the magnetization changed from canted antiferromagnetic spins between neighboring Fe^{3+} ions in $BiFe_{0.95}Co_{0.05}O_3$ to the ferrimagnetic spin arrangement between neighboring Fe^{3+} and Co^{3+} ions with increasing La^{3+} doping concentration.

Another interesting phenomenon is that La^{3+} substitution effectively decreases the coercivity. As shown in Fig. 5, the coercivity of $Bi(Fe_{0.95}Co_{0.05})O_3$ is 906 Oe. With increasing La substitution concentration, the coercivity decreases drastically to 344 Oe, 260 Oe, and 222 Oe for $(Bi_{1-x}La_x)(Fe_{0.95}Co_{0.05})O_3$ (x=0.10, 0.20, 0.30), respectively. For application, the coercivity should be smaller, so less power and simpler device structure are needed to switch the magnetization. To understand the mechanism, the initial magnetization curves are shown in Fig. 4. For the nucleation-type magnets the domain walls move freely inside the grains leading to steep increase in magnetization at low fields, while for pinning-type magnets the initial magnetization changes are very small for fields less than the sample coercivity because the domain walls are pinned [32]. As can be seen, a rather gradual increase of magnetization changes to a rather steep increase of magnetization at low field with increasing La^{3+} concentration, indicating the change of switching mode of magnetization from domain wall pinning to domain nucleation.

At room temperature, the polarization versus applied field (P–E) hysteresis loops for $(Bi_{1-x}La_x)(Fe_{0.95}Co_{0.05})O_3$ (x=0, 0.10, 0.20, 0.30) ceramics are shown in Fig. 6. The large leakage is still the main obstacles to observe the clear ferroelectric hysteresis loop and the P–E loops are not saturated under the highest voltage which can be applied. The P–E loop of $Bi(Fe_{0.95}Co_{0.05})O_3$ is round in shape, which is due to the large leakage current [33]. With increasing La doping level in $Bi(Fe_{0.95}Co_{0.05})O_3$, the shape of P–E loops were significantly improved. The improvement of the ferroelectric properties is due to the suppression of the leakage current [34], which would be ascribed to the suppression of the oxygen vacancies by La substitution for the volatile Bi [12]. The values of the remnant polarization (P_r) are 3.4 μC/cm², 4.2 μC/cm², 2.9 μC/cm² and 2.1 μC/cm² for

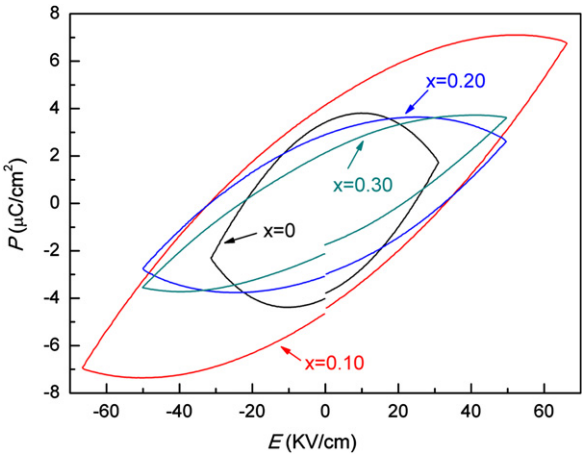

Fig. 6. The P–E hysteresis loops of $(Bi_{1-x}La_x)(Fe_{0.95}Co_{0.05})O_3$ ($x=0$, 0.10, 0.20, 0.30) ceramics.

$(Bi_{1-x}La_x)(Fe_{0.95}Co_{0.05})O_3$ ($x=0$, 0.10, 0.20, 0.30), respectively. As shown by XRD, the La substitution on Bi sites may suppress the formation of the secondary phases, leading to the decrease of the leakage current and improvement of the ferroelectricity. However, the degradation of the crystal anisotropy and the Curie temperature due to the La substitution might lead to the decrease of the remnant polarization [12]. The competition between these two effects leads to the observation of the maximum remnant polarization in $(Bi_{1-x}La_x)(Fe_{0.95}Co_{0.05})O_3$ with $x=0.10$. Though the theoretical calculation has predicted the giant polarization of 150 μC/cm^2 in tetragonal $BiFeO_3$, the experimental observation of the polarization hysteresis loop is rather rare and the observed value is much smaller [35]. We clearly observed the ferroelectricity in tetragonal La-doped $BiFe_{0.95}Co_{0.05}O_3$ ceramics. By optimizing the preparing condition, especially in high-quality films, the ferroelectric properties of tetragonal $((Bi_{1-x}La_x)(Fe_{0.95}Co_{0.05})O_3$ might be significantly improved. It should be noted that in tetragonal $BiFeO_3$, the polarization is aligned perpendicular to the collinear antiferromagnetic spins [29]. The clear ferroelectric and soft ferromagnetic properties were simultaneously observed in tetragonal $Bi_{0.70}La_{0.30}Fe_{0.95}Co_{0.05}O_3$, indicating the possible improved magnetoelectric coupling and potential multiferroic applications which needs further study.

4. Conclusions

In summary, La and Co co-doped $(Bi_{1-x}La_x)(Fe_{0.95}Co_{0.05})O_3$ ($x=0$, 0.10, 0.20, 0.30) ceramics have been prepared by tartaric acid modified sol–gel method. With increasing x, the structure changed from rhombohedral to tetragonal at $x=0.20$, which was confirmed by the XRD and Raman measurements. A drastic decrease of magnetization was observed with increasing x from 0 to 0.10, and increases with further increasing x to 0.30. The drop of magnetization has been attributed to the collinear antiferromagnetic spin structure in tetragonal phase, and the compensation of the La^{3+} and Co^{3+} co-doping on the lattice distortion. The increase of magnetization with $x \geq 0.10$ might be due to the ferrimagnetic spin arrangement between neighboring Fe^{3+} and Co^{3+} ions. With the competition between the reducing leakage current and the degradation of the crystal anisotropy and the Curie temperature by La substitution, the $Bi_{0.90}La_{0.10}Fe_{0.95}Co_{0.05}O_3$ shows the largest polarization. The clear observation of soft ferromagnetic and ferroelectric properties in tetragonal $Bi_{0.70}La_{0.30}Fe_{0.95}Co_{0.05}O_3$ indicates the potential multiferroic applications.

Acknowledgments

This work is supported by the National Natural Science Foundation of China (51172044), the National Science Foundation of Jiangsu Province of China (BK2011617), National Key Projects for Basic Researches of China (2010CB923404), by NCET-09–0296, the Scientific Research Foundation for the Returned Overseas Chinese Scholars, State Education Ministry, and Southeast University (the Excellent Young Teachers Program and Seujq201106).

References

[1] J. Wang, J.B. Neaton, H. Zheng, V. Nagarajan, S.B. Ogale, B. Liu, D. Viehland, V. Vaithyanathan, D.G. Schlom, U.V. Waghmare, N.A. Spaldin, K.M. Rabe, M. Wuttig, R. Ramesh, Science 299 (2003) 1719.
[2] N. Hur, S. Park, P.A. Sharma, J.S. Ahn, S. Guha, S.W. Cheong, Nature 429 (2004) 392.
[3] G. Catalan, J.F. Scott, Adv. Mater. 21 (2009) 2463.
[4] Y. Shuai, S. Zhou, S. Streit, H. Reuther, D. Bürger, S. Slesazeck, T. Mikolajick, M. Helm, H. Schmidt, Appl. Phys. Lett. 98 (2011) 232901.
[5] D. Lebeugle, D. Colson, A. Forget, M. Viret, P. Bonville, J.F. Marucco, S. Fusil, Phys. Rev. B. 76 (2007) 024116.
[6] I. Sosnowska, T. Peterlin-Neumaier, E. Steichele, J. Phys. C 15 (1982) 4835.
[7] C. Yang, J.S. Jiang, F.Z. Qian, D.M. Jiang, C.M. Wang, W.G. Zhang, J. Alloys Compd. 507 (2010) 29.
[8] H. Paik, H. Hwang, K. No, S. Kwon, D.P. Cann, Appl. Phys. Lett. 90 (2009) 042908.
[9] R.K. Mishra, D.K. Pradhan, R.N.P. Choudhary, A. Banerjee, J. Magn. Magn. Mater. 320 (2008) 2602.
[10] Y.P. Wang, L. Zhou, M.F. Zhang, X.Y. Chen, J.M. Liu, Z.G. Liu, Appl. Phys. Lett. 84 (2004) 1731.
[11] V.R. Palker, J. John, R. Pinto, Appl. Phys. Lett. 80 (2002) 1628.
[12] H. Uchida, R. Ueno, H. Funakubo, S. Kodo, J. Appl. Phys. 100 (2006) 014106.
[13] X.D. Qi, J. Dho, R. Tomov, M. Blamire, M.M. Driscoll, Appl. Phys. Lett. 86 (2005) 062903.
[14] M. Kumar, K.L. Yadav, J. Appl. Phys. 100 (2006) 074111.
[15] J. Allibe, I.C. Infante, S. Fusil, K. Bouzehouane, E. Jacquet, C. Deranlot, M. Bibes, A. Barthélémy, Appl. Phys. Lett. 95 (2009) 182503.
[16] V.S. Puli, A. Kumar, N. Panwar, I.C. Panwar, R.S. Katiyar, J. Alloys Compd. 509 (2011) 8223.
[17] Q. Xu, H. Zai, D. Wu, T. Qiu, M.X. Xu, Appl. Phys. Lett. 95 (2009) 112510.
[18] H. Naganuma, J. Miura, S. Okamura, Appl. Phys. Lett. 93 (2008) 052901.
[19] H. Naganuma, N. Shimura, J. Miura, H. Shima, S. Yasui, K. Nishida, T. Katoda, T. Iijima, H. Funakubo, S. Okamura, J. Appl. Phys. 103 (2008) 07E314.
[20] X.H. Zheng, Q.Y. Xu, Z. Wen, X.Z. Lang, D. Wu, T. Qiu, M.X. Xu, J. Alloys Compd. 499 (2010) 108.
[21] Q. Xu, H. Zai, D. Wu, Y.K. Tang, M.X. Xu, J. Alloys Compd. 485 (2009) 13.
[22] L.Y. Wang, D.H. Wang, H.B. Huang, Z.D. Han, Q.Q. Cao, B.X. Gu, Y.W. Du, J. Alloys Compd. 469 (2009) 1.
[23] Z.X. Cheng, A.H. Li, X.L. Wang, S.X. Dou, K. Ozawa, H. Kimura, S.J. Zhang, T.R. Shrout, J. Appl. Phys. 103 (2008) 07E507.
[24] D. Rout, K. Moon, S.L. Kang, J. Raman Spectrosc. 40 (2009) 618.
[25] J. Huang, Y. Shen, M. Li, C. Nan, J. Appl. Phys. 110 (2011) 094106.
[26] M. Naeem, S. Qaseen, I.H. Gul, A. Maqsood, J. Appl. Phys. 107 (2010) 124303.
[27] Q.Y. Xu, X.H. Zheng, Z. Wen, Y. Yang, D. Wu, M.X. Xu, Solid State Commun. 151 (2011) 624.
[28] R.D. Shannon, Acta Crystallogr., Sect. A: Found. Crystallogr. 32 (1976) 751.
[29] S. Bhattacharjee, A. Senyshyn, P.S.R. Krishna, H. Fuess, D. Pandey, Appl. Phys. Lett. 97 (2010) 262506.
[30] T. Stevenson, T.P. Comyn, A. Daoud-Aladine, A.J. Bell, J. Magn. Magn. Mater. 322 (2010) L64.
[31] J.J. Ge, X.B. Xue, G.F. Cheng, M. Yang, B. You, W. Zhang, X.S. Wu, A. Hu, J. Du, S.J. Zhang, S.M. Zhou, Z. Wang, B. Yang, L. Sun, J. Magn. Magn. Mater. 324 (2012) 200.
[32] M. Dospial, D. Plusa, B. Ślusarek, J. Magn. Magn. Mater. 324 (2012) 843.
[33] X. Zhang, Y. Sui, X. Wang, J. Mao, R. Zhu, Y. Wang, Z. Wang, Y. Liu, W. Liu, J. Alloys Compd. 509 (2011) 5908.
[34] X. Zhang, Y. Sui, X. Wang, Y. Wang, Z. Wang, J. Alloys. Compd. 507 (2010) 157.
[35] W. Chen, W. Ren, L. You, Y. Yang, Z. Chen, Y. Qi, X. Zou, J. Wang, T. Sritharan, P. Yang, L. Bellaiche, L. Chen, Appl. Phys. Lett. 99 (2011) 222904.